

Chapter 8

Transport

Abstract The physics of transport in semiconductors is treated foremost for charge transport. Band transport and scattering, mobility, low field and high field effects as well as polarons and hopping transport are covered. A short section mentions ionic transport before heat conduction and coupled heat and charge transport including thermopower and Peltier effect are discussed.

8.1 Introduction

Charge and heat energy can be transported through the semiconductor in the presence of appropriate (generalized) forces. Such a force can be an electric field or a temperature gradient. Both transport phenomena are coupled since electrons transport energy and charge simultaneously through the crystal. First, we will treat the charge transport as a consequence of a gradient in the Fermi level, then the heat transport upon a temperature gradient and finally the coupled system, i.e. the Peltier and Seebeck effects. Detailed treatments of carrier transport can be found in [631, 632].

Practically all important semiconductor devices are based on the transport of charge, such as diode, transistor, photodetector, solar cell and laser.

Carriers move in the semiconductor driven by a gradient in the Fermi energy. We distinguish

- drift, as a consequence of an electric field \mathbf{E} ,
- diffusion, as a consequence of a concentration gradient ∇n or ∇p .

In inhomogeneous semiconductors for which the position of the band edges is a function of position, another force occurs. This will not be treated here, since later (cf. Chap. 12) it will be included as an additional, internal electric field.

In Sects. 8.2–8.5 we treat band conductivity, i.e. the transport of charge carriers in extended states, the conduction and valence bands characterized by an effective mass. Conductivity is then determined by the carrier concentration (free electrons and holes) and scattering mechanisms (mobility). In disordered semiconductors such as amorphous material, the charge transport due to *hopping* between localized states close to the Fermi level dominates the conductivity which is discussed in Sect. 8.7.

Many semiconductor properties, such as the carrier concentration and the band gap, depend on the temperature. Thus, device properties will also depend on temperature. During operation of a device typically heat is generated, e.g. by Joule heating due to finite resistivity. This heat leads to an increase of the device temperature that subsequently alters the device performance, mostly for the worse. Ultimately, the device can be destroyed. Thus cooling of the device, in particular of the active area of the device, is essential. Mostly the thermal management of device heating limits the achievable performance (and lifetime) of the device. In high-power devices quite high energy densities can occur, e.g. the facet of a high-power semiconductor laser has to withstand an energy density beyond 10 MW cm^{-2} .

8.2 Conductivity

Under the influence of an electric field the electrons accelerate according to (cf. (6.32))

$$\mathbf{F} = m^* \frac{d\mathbf{v}}{dt} = \hbar \frac{d\mathbf{k}}{dt} = q \mathbf{E} = -e \mathbf{E}. \quad (8.1)$$

In the following, q denotes a general charge, while e is the (positive) elementary charge. We also consider an isotropic effective mass m^* at first. After the time δt the \mathbf{k} vector of all conduction electrons (and the center of the Fermi sphere) has been shifted by $\delta \mathbf{k}$

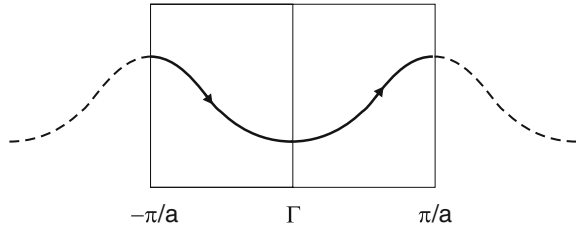
$$\delta \mathbf{k} = -\frac{e \mathbf{E}}{\hbar} \delta t. \quad (8.2)$$

In the absence of scattering processes this goes on further (similar to an electron in vacuum). This regime is called *ballistic* transport. In a (periodic) band structure, the electron will perform a closed cycle as indicated in Fig. 8.1. Such motion is called a Bloch oscillation. However, in a bulk crystal the period T of such an oscillation $eET/\hbar = 2\pi/a_0$ is of the order of 10^{-10} s for $E = 10^4$ V/cm. This time is much longer than a typical scattering time of 10^{-14} s. Thus, in bulk material the Bloch electron cannot reach the zone boundary. However, in artificial superlattices (cf. Chap. 12) with larger periodicity (≈ 10 nm), high electric fields ($\approx 10^6$ V/cm) and high quality (reduced collision time) such motion is possible. We note that in the absence of scattering, electrons also perform a periodic oscillation in a magnetic field (cyclotron motion).

In a real semiconductor, at finite temperatures, impurities, phonons and defects (finally also the surface) will contribute to scattering. In the relaxation-time approximation it is assumed that the probability for a scattering event, similar to friction, is proportional to the (average) carrier velocity. The average relaxation time τ is introduced via an additional term $\dot{\mathbf{v}} = -\mathbf{v}/\tau$ that sums up all scattering events.¹

¹Going beyond the relaxation time approximation is discussed in Sect. I.

Fig. 8.1 Schematic representation of a Bloch oscillation



Thus, the maximum velocity that can be reached in a static electric field is given by (steady-state velocity)

$$\mathbf{v} = -\frac{e \mathbf{E} \tau}{m^*}. \tag{8.3}$$

The current density per unit area is then linear in the field, i.e. fulfills Ohm’s law

$$\mathbf{j} = n q \mathbf{v} = \frac{n e^2 \mathbf{E} \tau}{m^*} = \sigma \mathbf{E}. \tag{8.4}$$

The conductivity σ in the relaxation-time approximation is given by

$$\sigma = \frac{1}{\rho} = \frac{n e^2 \tau}{m^*}. \tag{8.5}$$

In the case of a cylindrically symmetric mass such as for electrons in silicon or germanium, for the effective mass in (8.5) the effective conductivity mass must be used,

$$\frac{1}{m_\sigma^*} = \frac{1}{3} \left(\frac{2}{m_t} + \frac{1}{m_l} \right). \tag{8.6}$$

The specific resistivity is the inverse of the conductivity. Metals have a high conductivity (see Table 8.1), e.g. for Cu at room temperature $\sigma = 5.8 \times 10^5 \Omega^{-1} \text{cm}^{-1}$. At low temperatures (4 K) the conductivity is even a factor of 10^5 higher. The mean free path $d = \tau v_F$ is

$$d = \frac{\sigma m^* v_F}{n e^2}, \tag{8.7}$$

v_F being the Fermi velocity ($E_F = m^* v_F^2/2$). For copper, $d = 3 \text{ mm}$ at low temperature (and thus susceptible to the sample geometry) while at room temperature the mean free path is only about 40 nm. However, this becomes an issue when the metal line width and height of interconnects in integrated circuits approaches this length scale [633] (see Sect. 24.5.5).

In semiconductors, the carrier concentration depends strongly on the temperature. At zero temperature the conductivity is zero. Also, the scattering processes and thus the relaxation time constant exhibit a temperature dependence. The conductivity spans a large range from insulating to almost metallic conduction (see Table 8.1).

Table 8.1 Conductivity at room temperature for various metals, semiconductors, insulators and liquids

Material	σ ($\Omega^{-1} \text{ cm}^{-1}$)
Ag	6.25×10^5
Al	3.6×10^5
Au	4.35×10^5
Cu	5.62×10^5
Fe	1.1×10^5
Pt	1.02×10^5
Ge pure ($N_D \sim 10^{13} \text{ cm}^{-3}$)	10^{-2}
Ge ($N_D \sim 10^{15} \text{ cm}^{-3}$)	1
Ge ($N_D \sim 10^{17} \text{ cm}^{-3}$)	2×10^1
Ge ($N_D \sim 10^{18} \text{ cm}^{-3}$)	2×10^2
Si pure	4.5×10^{-6}
Si:As ($N_D \sim 3 \times 10^{19} \text{ cm}^{-3}$)	4×10^2
Si:B ($N_A \sim 1.5 \times 10^{19} \text{ cm}^{-3}$)	1.2×10^2
GaAs pure	1.4×10^{-7}
ZnO:Al (highly doped)	$\approx 1 \times 10^4$
Pentacene	$10^{-8} - 10^{-4}$
SiO ₂	$\approx 10^{-15}$
Al ₂ O ₃	$\approx 10^{-16}$
H ₂ O pure	4×10^{-8}
Hexane	$\approx 10^{-18}$

8.3 Low-Field Transport

First we consider only *small* electric fields. The real meaning of this will only become clear in Sect. 8.4 on high-field transport. In the low-field regime the velocity is proportional to the electric field.

8.3.1 Mobility

The mobility is defined (scalar terms) as

$$\mu = \frac{v}{E}. \quad (8.8)$$

By definition, it is a negative number for electrons and positive for holes. However, the numerical value is usually given as a positive number for both carrier types. In an intrinsic semiconductor the mobility is determined by scattering with phonons.

Table 8.2 Mobilities of electrons and holes at room temperature for various semiconductors

Material	$-\mu_n(\text{cm}^2/\text{Vs})$	$\mu_p(\text{cm}^2/\text{Vs})$
Si	1300	500
Ge	4500	3500
GaAs	8800	400
GaN	300	180
InSb	77 000	750
InAs	33 000	460
InP	4600	150
ZnO	230	8

Further scattering is introduced by impurities, defects or alloy disorder. The conductivity is (8.4)

$$\sigma = q n \mu \tag{8.9}$$

for each carrier type. Using (8.5) the mobility in the relaxation time approximation is

$$\mu = \frac{q \tau}{m^*}. \tag{8.10}$$

In the presence of both electrons and holes,

$$\sigma = \sigma_e + \sigma_h = -e n \mu_n + e p \mu_p, \tag{8.11}$$

where μ_n and μ_p are the mobilities for electrons and holes, respectively. These are given by $\mu_n = -e \tau_n / m_e^*$ and $\mu_p = e \tau_p / m_p^*$.

As the unit for mobility, usually cm^2/Vs is used. While Cu at room temperature has a mobility of $35 \text{ cm}^2/\text{Vs}$, semiconductors can have much higher values. In two-dimensional electron gases (cf. Chap. 12), the mobility can reach several $10^7 \text{ cm}^2/\text{Vs}$ at low temperature (Fig. 12.36). In bulk semiconductors with small band gap, a high electron mobility is caused by its small effective mass. Some typical values are given in Table 8.2.

8.3.2 Microscopic Scattering Processes

The relaxation time constant summarizes all scattering mechanisms. If the relaxation times τ_i of various processes are independent, the Matthiessen rule can be used to obtain the mobility ($\mu_i = q \tau_i / m^*$)

$$\frac{1}{\mu} = \sum_i \frac{1}{\mu_i}. \tag{8.12}$$

The various scattering mechanisms have quite different temperature dependences such that the mobility is a rather complicated function of temperature. In [634] the mechanisms determining the low and high-field transport properties of (cubic) semiconductors are reviewed.

8.3.3 Ionized Impurity Scattering

Theoretically, this problem is treated similar to Rutherford scattering. A screened Coulomb potential is assumed, as the scattering potential

$$V(r) = -\frac{Z e}{4\pi\epsilon_0\epsilon_r} \frac{1}{r} \exp\left(-\frac{r}{l_D}\right), \quad (8.13)$$

where l_D is the screening length. The problem has been treated classically by Conwell and Weisskopf [635] and quantum mechanically by Brooks [636] and Herring. An expression for the mobility that encompasses the Conwell–Weisskopf and Brooks–Herring results is derived in [637]. Further details are given in [638, 639]. For the mobility it is found that

$$\mu_{\text{ion.imp.}} = \frac{2^{7/2} (4\pi\epsilon_0\epsilon_r)^2 (kT)^{3/2}}{\pi^{3/2} Z^2 e^3 \sqrt{m^*}} \frac{1}{N_{\text{ion}}} \frac{1}{\ln(1+b) - 1/(1+1/b)}, \quad (8.14)$$

with $b = 4(k/l_D)^2 = 8m^* E (l_D/\hbar)^2$. In the Thomas–Fermi screening model

$$l_D^2 = 4\pi \frac{e^2}{\epsilon_0\epsilon_r} N(E_F) = \left(\frac{3}{\pi}\right)^{1/3} \frac{4m^* e^2}{\epsilon_0\epsilon_r \hbar^2} n^{1/3}. \quad (8.15)$$

The formula (8.14) is valid only for $b \gg 1$, i.e. small carrier densities. A similar formula from [638] is

$$\mu_{\text{ion.imp.}} = \frac{128\sqrt{2\pi} (\epsilon_0\epsilon_r)^2 (kT)^{3/2}}{m^{*1/2} Z^2 N_{\text{ion}} e^3} \left[\ln \frac{24m^* \epsilon_0\epsilon_r (kT)^2}{n e^2 \hbar^2} \right]^{-1}. \quad (8.16)$$

For large ionized impurity (and carrier) density ($b \ll 1$), the mobility is given by [483]

$$\mu_{\text{ion.imp.}} = \frac{4e}{3^{1/3} \pi^{2/3} \hbar} n^{-2/3}, \quad (8.17)$$

the value of the pre-factor being about $3 \times 10^{14} (\text{Vs})^{-1}$.

The scattering time depends like $\tau \propto (E/kT)^s$ on the kinetic energy; for moderate or weak scattering $s = 3/2$, for very strong scattering, $s = -1/2$ [632].

For typical substitutional impurities, the charge of the scattering center is $|Z| = 1$; in oxides, oxygen vacancies may have $Z = 2$. At high impurity densities, impurity

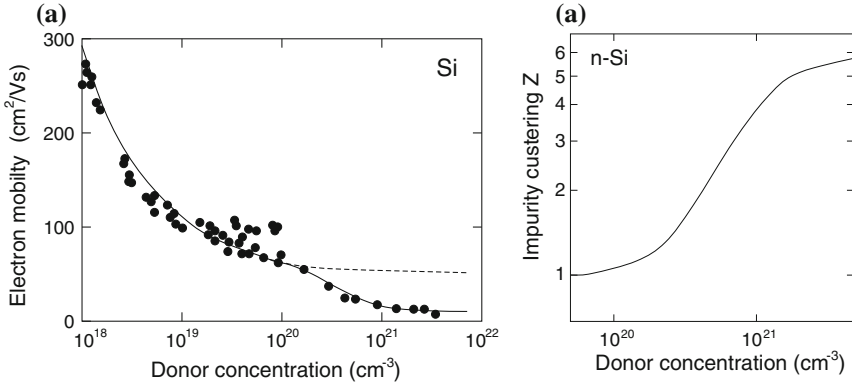


Fig. 8.2 (a) Electron mobility in highly doped silicon. Experimental data (*symbols*) from various sources and modeling with ionized impurity scattering with (*solid line*) and without (*dashed line*) considering impurity clustering. (b) Effective impurity cluster charge Z_D . Adapted from [640]

clusters may form with $|Z| > 1$; this will have a strong influence on the scattering rate since it is proportional to Z^2 . The decrease of mobility for $N_D > 10^{20} \text{ cm}^{-3}$ (Fig. 8.2a) is attributed to such effect which can be described with an effective impurity clustering charge Z_D (Fig. 8.2b) [640, 641].

8.3.4 Deformation Potential Scattering

Acoustic phonons with small wavevector, i.e. a wavelength large compared to the unit cell, can have TA or LA character. The TA phonons represent a shear wave (with zero divergence), the LA phonons are a compression wave (with zero rotation). The LA is a plane wave of displacement $\delta \mathbf{R}$ parallel to the k -vector \mathbf{q} ,

$$\delta \mathbf{R} = \mathbf{A} \sin (\mathbf{q} \cdot \mathbf{R} - \omega t) . \tag{8.18}$$

The strain tensor is given by

$$\epsilon_{ij} = \frac{1}{2} (\mathbf{q}_i \mathbf{A}_j + \mathbf{q}_j \mathbf{A}_i) \cos (\mathbf{q} \mathbf{R} - \omega t) . \tag{8.19}$$

It has a diagonal form $\epsilon_{ij} = \mathbf{q}_i \mathbf{A}_j$ for \mathbf{q} and $\omega \rightarrow 0$. Therefore, the LA phonon creates an oscillatory volume dilatation (and compression) with amplitude $\mathbf{q} \cdot \mathbf{A}$. This volume modulation affects the position of the band edges. For the conduction-band edge the energy change is related to the volume change by the hydrostatic deformation potential $E_{ac,def.} = V \partial E_C / \partial V$. Since the modulation is small compared to the energy of the charge carriers, it is mostly an elastic scattering process. The Hamilton operator for the LA scattering is

$$\hat{H} = E_{\text{ac.def.}} (\mathbf{q} \cdot \mathbf{A}). \quad (8.20)$$

The size of the LA amplitude is given by the number of phonons in the mode that is given by the Bose–Einstein distribution, $N_{\text{ph}}(\hbar\omega) = [\exp(\frac{\hbar\omega}{kT})]^{-1}$. The mobility due to acoustic deformation potential scattering is found to be

$$\mu_{\text{ac.def.}} = \frac{2\sqrt{2\pi} e \hbar^4 c_1}{3 m^{*5/2} E_{\text{ac.def.}}^2} (kT)^{-3/2}, \quad (8.21)$$

where $c_1 = \rho c_s^{\text{LA}}$, ρ being the density and c_s being the sound velocity. The scattering time increases like $\tau \propto E^{-1/2}$ with the kinetic energy [632].

The acoustical deformation potential scattering is important at high temperatures. It is dominating in nonpolar semiconductors (Ge, Si) at high temperatures (typically at and above room temperature).

8.3.5 Piezoelectric Potential Scattering

In piezoelectric crystals (see Sect. 15.4), i.e. crystals that show an electric polarization upon strain, certain acoustic phonons lead to piezoelectric fields. In GaAs, with $\langle 111 \rangle$ being the piezoelectric directions, this is the case for shear waves. In strongly ionic crystals, e.g. II–VI semiconductors, the piezoelectric scattering can be stronger than the deformation potential scattering. The mobility due to piezoelectric potential scattering is

$$\mu_{\text{pz.el.}} = \frac{16\sqrt{2\pi}}{3} \frac{\hbar \epsilon_0 \epsilon_r}{m^{*3/2} e K^2} (kT)^{-1/2}, \quad (8.22)$$

with $K = \frac{e_p^2/c_1}{\epsilon_0 \epsilon_r + e_p^2/c_1}$, e_p being the piezoelectric coefficient.

8.3.6 Polar Optical Scattering

LO phonons are connected with an electric field antiparallel to the displacement (5.52). In the scattering mechanism the absorbed or emitted phonon energy $\hbar\omega_0$ is comparable to the thermal energy of the carriers. Therefore, the scattering is inelastic and the relaxation-time approximation does not work. The general transport theory is complicated. If the temperature is low compared to the Debye temperature, $T \ll \Theta_D$

$$\mu_{\text{pol.opt.}} = \frac{e}{2 m^* \alpha \omega_0} \exp\left(\frac{\Theta_D}{T}\right), \quad (8.23)$$

where $\alpha = \frac{1}{137} \sqrt{\frac{m^* c^2}{2k\Theta_D}} \left(\frac{1}{\epsilon(\infty)} - \frac{1}{\epsilon(0)} \right)$ is the dimensionless polar constant.

8.3.7 Dislocation Scattering

Dislocations can contain charge centers and thus act as scattering centers [642]. This has been first demonstrated for n-Ge crystals that have been deformed [643, 644]. The deformation has introduced acceptor-type defects reducing the mobility in particular at low temperatures (similar to ionized impurity scattering). The mobility due to dislocation scattering in an n-type semiconductor is given by [645, 646]

$$\mu_{\text{disl.}} = \frac{30 \sqrt{2\pi} \epsilon^2 d^2 (kT)^{3/2}}{N_{\text{disl}} e^3 f^2 L_D \sqrt{m^*}} \propto \frac{\sqrt{n}}{N_{\text{disl}}} T, \quad (8.24)$$

d being the average distance of acceptor centers along the dislocation line, f their occupation rate, N_{disl} the area density of dislocations and $L_D = (\epsilon kT / (e^2 n))^{1/2}$ the Debye screening length. The relation $\mu \propto \sqrt{n} / N_{\text{disl}}$ has been confirmed for various n-type GaN samples [647].

8.3.8 Grain Boundary Scattering

The lowering of mobility due to transport across grain boundaries is an important effect in polycrystalline materials, such as poly-silicon for solar cells or thin film transistors [648–651]. Grain boundaries contain electronic traps whose filling depends on the doping of the bulk of the grains. Charges will be trapped in the grain boundaries and a depletion layer will be created.² At low doping the grains are fully depleted and all free carriers are trapped in the grain boundaries. This means low conductivity, however, no electronic barrier to transport exists. At intermediate doping, traps are partially filled and the partial depletion of the grain leads to the creation of an electronic barrier ΔE_b (Fig. 8.3a) hindering transport since it must be overcome via thermionic emission. At high doping the traps are completely filled and the barrier vanishes again. Accordingly the mobility goes through a minimum as a function of the doping concentration (Fig. 8.3b) [648]. In [652] these data have been modeled with a 20 nm grain size, the value found in [648] from TEM analysis.

²The following arguments may only be followed once the concept of depletion layers and band bending is understood, see Sect. 21.2.1.

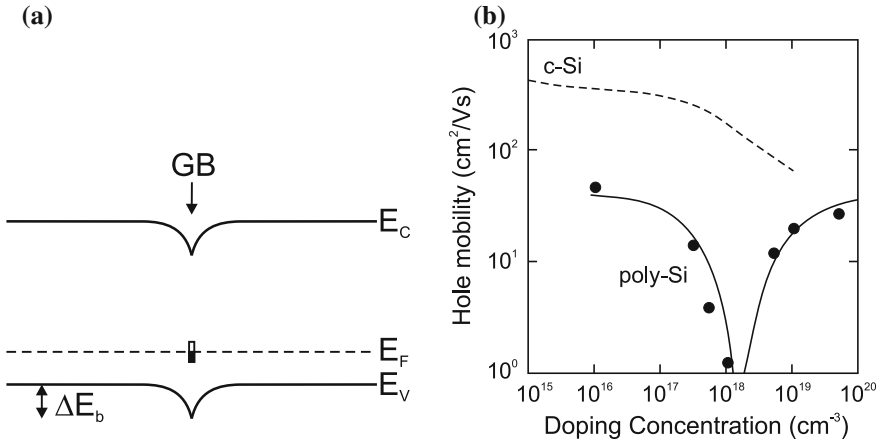


Fig. 8.3 (a) Electronic barrier (ΔE_b) for (hole) transport at a grain boundary (GB). (b) Average hole mobility in poly-silicon, experimental data (*symbols*) and theoretical model (*solid line*). The dependence for monocrystalline silicon is shown for comparison as *dashed line*. Adapted from [648]

The expression for the limitation of the mobility due to scattering at grain boundaries is given by [651, 653]

$$\mu_{GB} = \frac{e L_G}{\sqrt{8m^* \pi k}} T^{-1/2} \exp\left(-\frac{\Delta E_b}{kT}\right), \quad (8.25)$$

where L_G is the grain size.

8.3.9 Temperature Dependence

The sum of all scattering processes leads to a fairly complicated temperature dependence of the mobility $\mu(T)$. In covalent semiconductors (Si, Ge) the most important processes are the ionized impurity scattering ($\mu \propto T^{3/2}$) at low temperatures and the deformation potential scattering ($\mu \propto T^{-3/2}$) at high temperatures (Fig. 8.4a). In polar crystals (e.g. GaAs) at high temperatures the polar optical scattering is dominant (Fig. 8.4b).

In Fig. 8.5 the electron mobility of bulk and thin-film ZnO is compared. Since ZnO is polar the mobility at room temperature is limited by polar optical phonon scattering. In the thin film, grain-boundary scattering (Sect. 8.3.8) additionally occurs and limits the mobility.

Since the carrier concentration increases with increasing temperature and the mobility decreases, the conductivity has a maximum, typically around 70 K

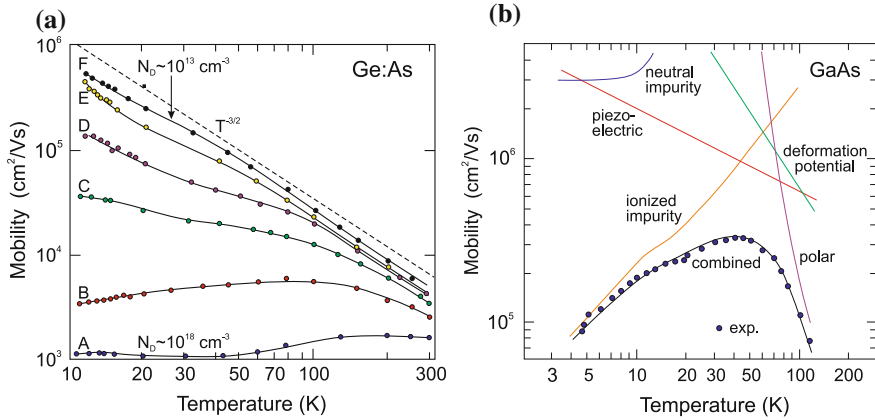


Fig. 8.4 (a) Temperature dependence of the electron mobility in n-doped Ge (for various doping levels from $N_D \approx 10^{18}$ for sample A to 10^{13} cm^{-3} for sample F in steps of a factor of ten). *Dashed line* indicates $T^{-3/2}$ dependence of deformation potential scattering, *solid lines* are guides to the eye. Adapted from [515]. (b) $\mu_n(T)$ for n-type GaAs ($N_D \approx 5 \times 10^{13} \text{ cm}^{-3}$, $N_A \approx 2 \times 10^{13} \text{ cm}^{-3}$). *Solid lines* are theoretical mobilities for various scattering mechanisms and combined mobility according to (8.12). Adapted from [654]

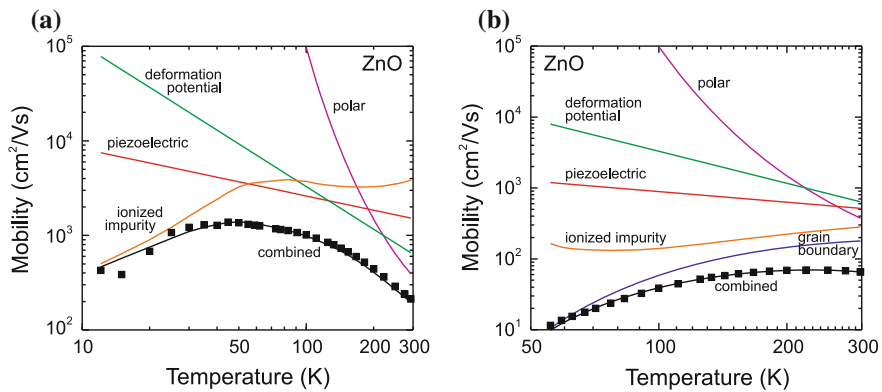


Fig. 8.5 Temperature dependence of the electron mobility in n-type (a) bulk ZnO and (b) a PLD-grown ZnO thin film on sapphire. In the latter, grain-boundary scattering is limiting the mobility. *Squares* are experimental data, *solid lines* are theoretical mobilities for various scattering mechanisms and combined mobility according to (8.12). Experimental data from [655]

(see Fig. 8.6). At very high temperature, when intrinsic conduction starts, σ shows a strong increase due to the increase in n .

At low temperature, the disorder due to doping (random positions of the impurity atoms) leads to a temperature driven metal–insulator transition as depicted in Fig. 7.29.

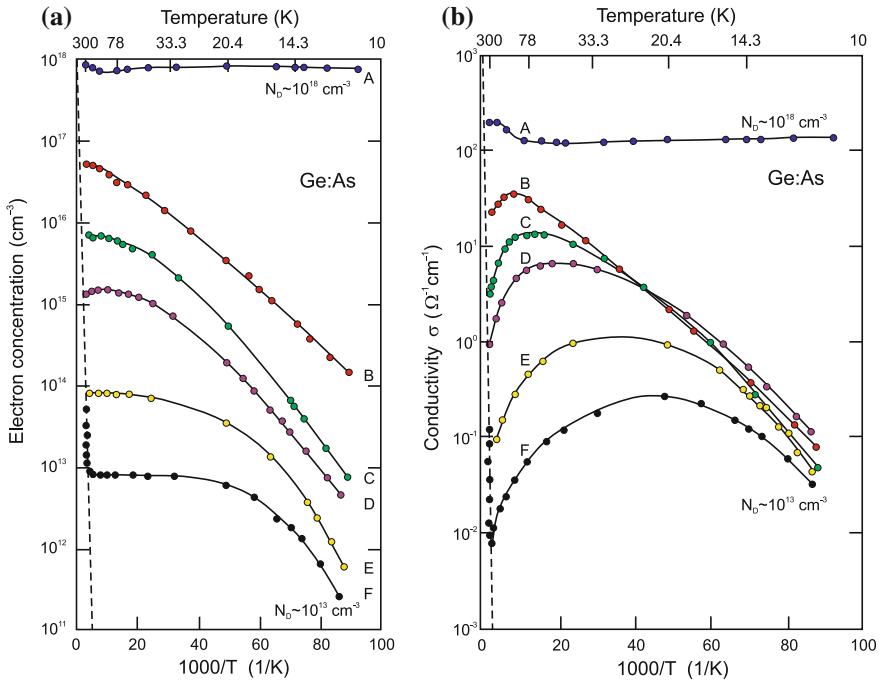


Fig. 8.6 (a) Carrier concentration and (b) conductivity of n-type Ge as a function of temperature. The doping level varies from $N_D \approx 10^{13}$ – 10^{18} (samples A–F as in Fig. 8.4a where the mobility of the same samples is shown). The *dashed lines* are for intrinsic Ge. The *solid lines* are guides to the eye. Adapted from [515]

8.3.10 Doping Dependence

The mobility decreases with increasing dopant concentration as already shown in Figs. 8.2 and 8.4a. In Fig. 8.7a the low doping limit is due to deformation potential scattering; the decrease with doping is due to ionized impurity scattering. At high doping level, it becomes more important at room temperature than (acoustical or optical) phonon scattering [656]. The mobility of carriers in n- and p-type silicon with very high carrier concentrations is depicted in Fig. 8.7b.

Thus, for bulk material high carrier density and high mobility are contrary targets and cannot be achieved simultaneously. A solution will be provided with the concept of *modulation doping* where the dopants and the (two-dimensional) carrier gas will be spatially separated in a heterostructure (cf. Sect. 12.3.4).

At high doping, the substitutional character of the impurities may be lost and secondary phases can arise, e.g. as observed for highly doped ZnO:Ga, exhibiting octahedral coordination of gallium in a parasitic ZnGa_2O_4 spinel phase for $[\text{Ga}] = 4\%$ [553]. The onset of such segregation phenomena is accompanied with the decrease of mobility and conductivity.

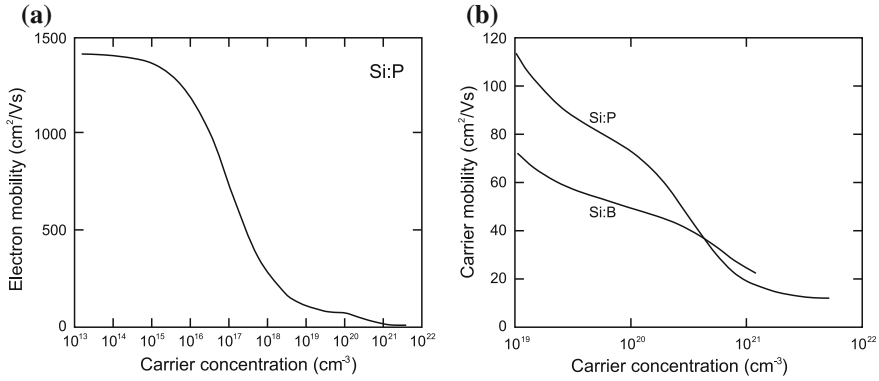


Fig. 8.7 (a) Electron mobility in Si:P at room temperature over a wide range of carrier concentrations. (b) Electron mobility in Si:P and hole mobility in Si:B for various high carrier concentrations. Adapted from [657]

8.3.11 Piezoresistivity

The dependence of resistivity on stress or strain is known as piezoresistive effect, first described in [658]. It is a consequence of the modification of the band structure upon stress and the change of effective masses (Sect. 6.10.2). In a cubic material, the resistivity ρ_i for transport in cartesian direction i changes compared to the unstrained state in a phenomenological description according to

$$\frac{\Delta\rho_i}{\rho_i} = \pi_{ij} \sigma_j, \tag{8.26}$$

where π is the piezoresistivity tensor (8.27) and the σ_j form the six-component stress tensor (5.59),

$$\pi = \begin{pmatrix} \pi_{11} & \pi_{12} & \pi_{12} & 0 & 0 & 0 \\ \pi_{12} & \pi_{11} & \pi_{12} & 0 & 0 & 0 \\ \pi_{12} & \pi_{12} & \pi_{11} & 0 & 0 & 0 \\ 0 & 0 & 0 & \pi_{44} & 0 & 0 \\ 0 & 0 & 0 & 0 & \pi_{44} & 0 \\ 0 & 0 & 0 & 0 & 0 & \pi_{44} \end{pmatrix}. \tag{8.27}$$

Values for the piezoelectric coefficients are given in Table 8.3 for Si, Ge and GaAs.

The piezoelectric effect has been discussed in detail [659] and modeled for p-type Si [660]. We shall only give a simple example which is particularly relevant for advanced CMOS design (Sect. 24.5.5); the directional dependence of the piezoresistive coefficient of silicon is shown for uniaxial stress within in the (001) plane in Fig. 8.8. Uniaxial tensile stress increases hole resistivity along $\langle 110 \rangle$ stress directions, compressive stress thus increases hole conductivity.

Table 8.3 Piezoresistivity coefficients (in 10^{-11} Pa^{-1}) for Si, Ge and GaAs at room temperature

Material	ρ ($\Omega \text{ cm}$)	π_{11}	π_{12}	π_{44}	Reference
p-Si	7.8	6.6	-1.1	138.1	[658]
n-Si	11.7	-102.2	53.4	-13.6	[658]
p-Ge (Ge:Ga)	15.0	-10.6	5.0	98.6	[658]
n-Ge (Ge:As)	9.9	-4.7	-5.0	-137.9	[658]
p-GaAs	$\sim 10^{-3}$	-12.0	-0.6	46	[662]
n-GaAs	$\sim 10^{-3}$	-3.2	-5.4	-2.5	[662, 663]

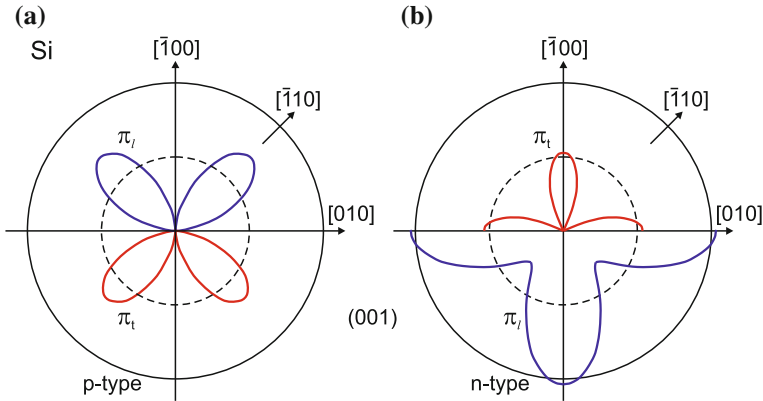


Fig. 8.8 Piezoresistive coefficient for current parallel (perpendicular) to the stress π_t as blue lines (π_l , red lines) for uniaxially stressed Si (001) at room temperature, (a) for p-type Si, (b) for n-type Si. The upper (lower) halves of the graphs show positive (negative) values of the piezoresistive coefficient, i.e. resistivity increases (decreases) with tensile stress. The solid circle indicates the value of $|\pi| = 10^{-9} \text{ Pa}^{-1}$, the dashed circle half that value. Adapted from [661]

8.4 High-Field Transport

In the case of small electric fields the scattering events are elastic. The drift velocity is linearly proportional to the electric field. The average thermal energy is close to its thermal value $3kT/2$ and the carriers are close to their band edges (Fig. 8.9a). The scattering efficiency, however, is reduced already at moderate fields. Then, the electron temperature [664] becomes larger than the lattice temperature. With increasing electrical field the carriers can gain more and more energy and will on average populate higher states, assuming a non-Boltzmann (and non-Fermi) statistical distribution [665]. The electron distribution in \mathbf{k} -space is depicted for silicon for three different electric fields in Fig. 8.9b,c. Hot carriers suffer additional scattering processes that are discussed in the following, namely optical phonon emission, intervalley scattering and impact ionization.

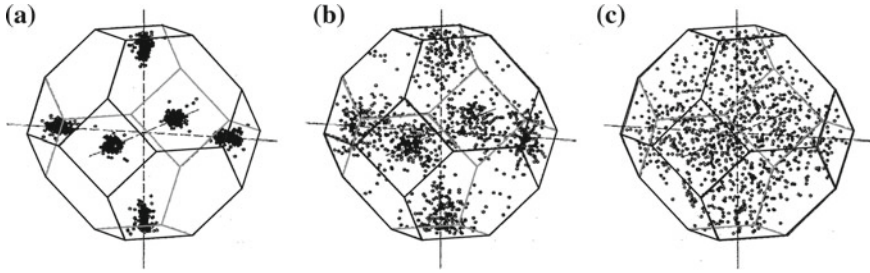


Fig. 8.9 Distribution of electrons in silicon in momentum space (cmp. Fig. 6.29c) for electric fields of (a) 10 kV/cm, (b) 10^2 kV/cm and (c) 10^3 kV/cm. Adapted from [665]

8.4.1 Drift-Saturation Velocity

If the carrier energy is large enough it can transfer energy to the lattice by the emission of an optical phonon. This mechanism is very efficient and limits the maximum drift velocity. Such behavior is non-ohmic. The limiting value for the drift velocity is termed the *drift-saturation velocity*. It is given by [666]

$$v_s = \sqrt{\frac{8}{3\pi}} \sqrt{\frac{\hbar\omega_{LO}}{m^*}}. \quad (8.28)$$

This relation can be obtained from an energy-balance consideration. The energy gain per unit time in the electric field is equal to the energy loss by the emission of an optical phonon.

$$q \mathbf{v} \cdot \mathbf{E} = \frac{\hbar\omega_{LO}}{\tau}, \quad (8.29)$$

where τ is the typical relaxation time constant for LO phonon emission. Together with (8.3) we find (8.29) except for the pre-factor, which is close to 1. The exact pre-factor results from a more exact quantum-mechanical treatment. For Ge the drift-saturation velocity at room temperature is 6×10^6 cm/s, for Si it is 1×10^7 cm/s (Fig. 8.10a). The carrier velocity also depends on the crystallographic direction [667].

8.4.2 Negative Differential Resistivity

In GaAs there is a maximum drift velocity of about 2×10^7 cm/s and following a reduction in velocity with increasing field (1.2×10^7 cm/s at 10 kV/cm, 0.6×10^7 cm/s at 200 kV/cm) as shown in Fig. 8.10a. This regime, above the threshold field of $E_{thr} = 3.2$ kV/cm in GaAs, is called *negative differential resistivity* (NDR) and was predicted in [673]. This phenomenon can be used in microwave oscillators, e.g. the Gunn element (Sect. 21.5.11).

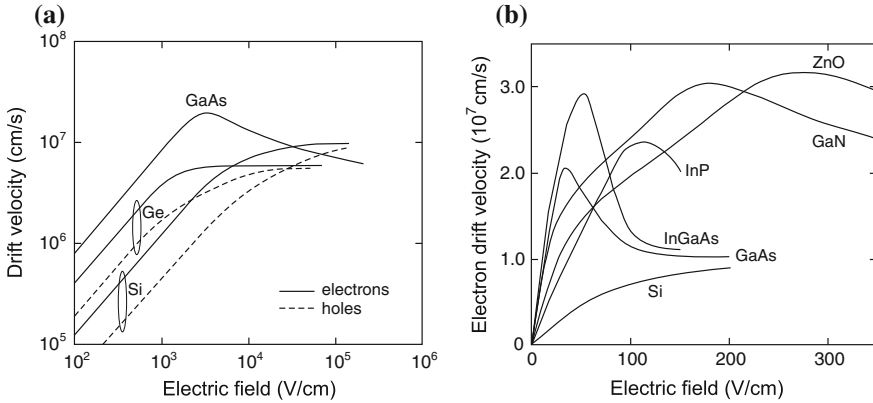


Fig. 8.10 Drift velocity at room temperature as a function of applied electric field for (a) high-purity Si, Ge, and GaAs on a double-logarithmic plot and (b) on linear plots for Si [668], Ge [669], GaAs [598], InP [670], InGaAs [671], GaN and ZnO [672]

Table 8.4 Material parameters for multivalley bandstructure of GaAs and InP

Material	E_g (eV)	ΔE (eV)	E_{thr} (kV/cm)	v_p (10^7 cm/s)	Lower valley (Γ)		Upper valley (L)	
					m^* (m_0)	μ_n (cm^2/Vs)	m^* (m_0)	μ_n (cm^2/Vs)
GaAs	1.42	0.36	3.2	2.2	0.068	≈ 8000	1.2	≈ 180
InP	1.35	0.53	10.5	2.5	0.08	≈ 5000	0.9	≈ 100

ΔE denotes the energetic separation of the two lowest valleys of the conduction band, E_{thr} the threshold field for NDR and v_p the peak velocity (at E_{thr}). Most values from [675]

The effect occurs in a multivalley band structure (see Fig. 8.11, for values cf. Table 8.4), e.g. in GaAs or InP, when the carrier energy is high enough to scatter (Fig. 8.11c, d) from the Γ minimum (small mass and high mobility) into the L valley (large mass and low mobility) [674].

The temperature dependence of the saturation velocity is shown in Fig. 8.12. With increasing temperature the saturation velocity decreases since the coupling with the lattice becomes stronger.

8.4.3 Velocity Overshoot

When the electric field is switched on, the carriers are at first in the Γ minimum (Fig. 8.11a). Only after a few scattering processes are they scattered into the L minimum. This means that in the first moments transport occurs with the higher mobility of the lowest minimum (Fig. 8.11e). The velocity is then larger than the (steady-state) saturation velocity in a dc field. This phenomenon is called *velocity overshoot* and is

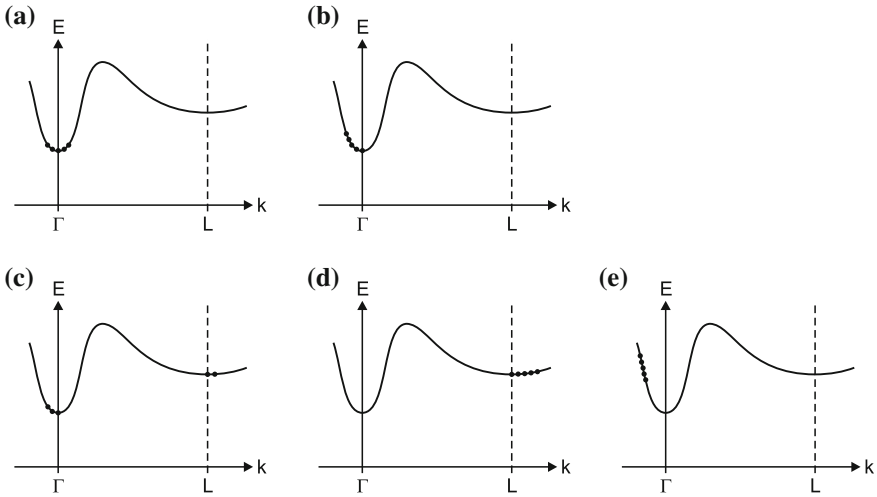
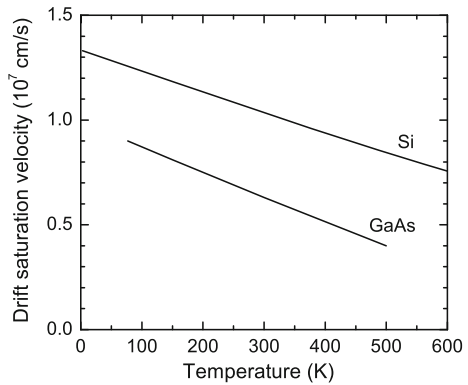


Fig. 8.11 Charge-carrier distribution in a multivalley band structure (e.g. GaAs, InP) for (a) zero, (b) small ($E < E_a$), (c) intermediate and (d) large ($E > E_b$) field strength. The situation shown in (e) is reached temporarily during velocity overshoot (see also Fig. 8.13)

Fig. 8.12 Temperature dependence of the saturation velocity for Si (following $v_s = v_{s0} (1 + 0.8 \exp(T/600\text{K}))^{-1}$ with $v_{s0} = 2.4 \times 10^7$ cm/s from [668]) and GaAs [598, 676, 677]

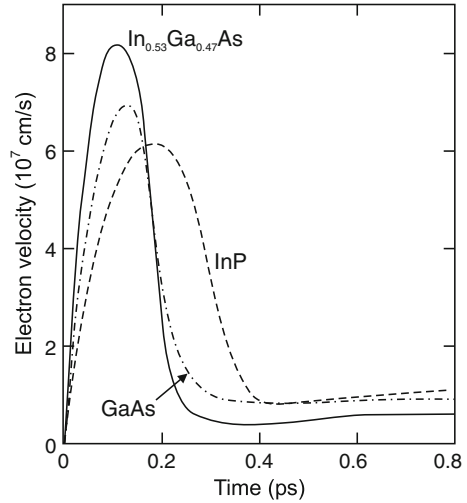


a purely dynamic effect (Fig. 8.13). Velocity overshoot in GaN is discussed in [678]. It is an important effect in small transistors.

8.4.4 Impact Ionization

If the energy gain in the field is large enough to generate an electron–hole pair, the phenomenon of impact ionization occurs. The kinetic energy is $\propto v^2$. Momentum and energy conservation apply. Thus, at small energies (close to the threshold for impact ionization) the vectors are short and collinear to fulfill momentum conservation. At

Fig. 8.13 Time dependence of the electron velocity at room temperature upon a step-like electric field (40kV/cm) for GaAs (dash-dotted line), InP (dashed line) and $\text{In}_{0.53}\text{Ga}_{0.47}\text{As}$ (solid line)



higher energy, larger angles between the velocity vectors of the impact partners can also occur. If the process is started by an electron (Fig. 8.14a) the threshold energy is given by [679]

$$E_e^{\text{thr}} = \left(1 + \frac{m_e}{m_e + m_{\text{hh}}}\right) E_g. \quad (8.30)$$

If the process starts with a heavy hole, the threshold [679],

$$E_{\text{hh}}^{\text{thr}} = \left(1 + \frac{m_{\text{hh}}}{m_e + m_{\text{hh}}}\right) E_g, \quad (8.31)$$

is larger because of the larger hole mass.

The threshold for impact ionization triggered by a split-off hole (shown schematically in Fig. 8.14b) is [680]

$$E_h^{\text{thr}} = \left(1 + \frac{m_{\text{so}}(1 - \Delta_0/E_g)}{2m_{\text{hh}} + m_e - m_{\text{so}}}\right) E_g. \quad (8.32)$$

Thus so-holes have typically the smaller threshold.³ At energies where impact ionization occurs, non-parabolicities are typically important, thus (8.30)–(8.32) are only indicative. The threshold behavior and the dependence of the scattering rate as a function of the primary carrier energy in Si, calculated considering the detailed band structure, is shown in Fig. 8.15.

³ Assuming $m_{\text{so}} = m_e$, $m_e \ll m_{\text{hh}}$ and $\Delta_0 \ll E_g$, $E_{\text{so}}^{\text{thr}}/E_e^{\text{thr}} \approx 1 - (m_e/m_{\text{hh}})(1 + \Delta_0/E_g)/2 < 1$.

Fig. 8.14 Electron and hole transitions for impact ionization close to the threshold energy. Ionization is triggered by (a) an electron and (b) a split-off hole of velocity v_i

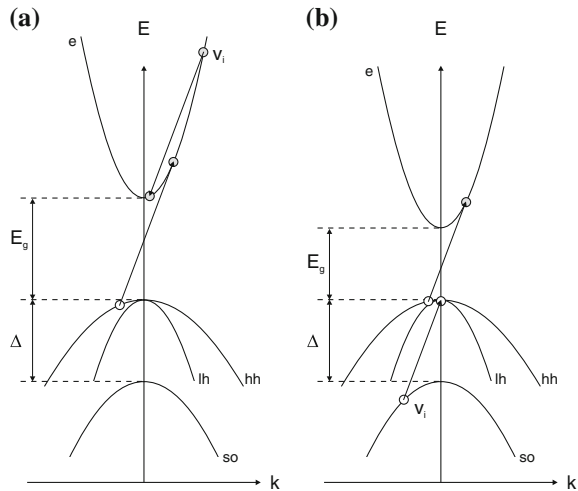
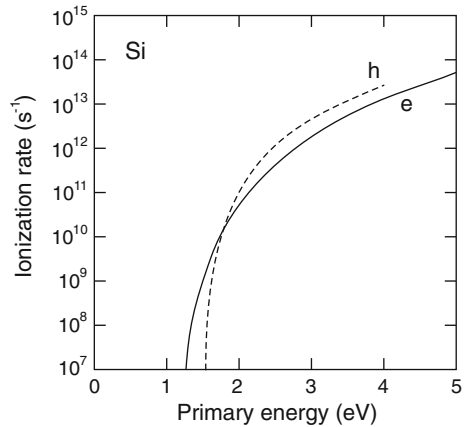


Fig. 8.15 Impact ionization rate as a function of primary carrier energy for electrons (solid line) and holes (dashed line) in silicon at room temperature. The curves are fit to results from a Monte-Carlo simulation. Adapted from [681, 682]



The generation rate G of electron–hole pairs during impact ionization is given by

$$G = \alpha_n n v_n + \alpha_p p v_p, \tag{8.33}$$

where α_n is the electron ionization coefficient. It describes the generation of electron–hole pairs per incoming electron per unit length. α_p denotes the hole ionization coefficient. The coefficients depend strongly on the applied electric field. They are shown in Fig. 8.16. They also depend on the crystallographic direction.

The impact ionization initiated by electrons and holes in silicon has been calculated considering the full band structure using a Monte Carlo technique in [681] and [682], respectively. In both cases the impact ionization rate is anisotropic for excess energies smaller than 3 eV and become isotropic above. The average energies

Fig. 8.16 Impact ionization rates for electrons and holes as a function of the inverse electric field for Si, Ge and other compound semiconductors at 300 K. Adapted from [500]

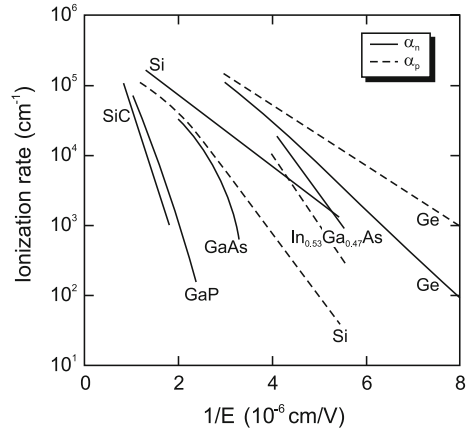
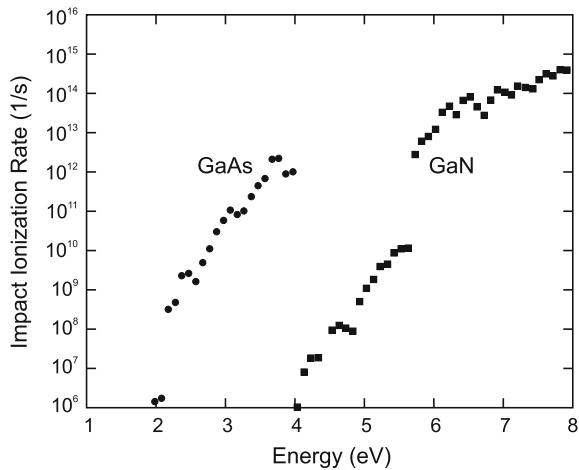


Fig. 8.17 Averaged rates for electron initiated impact ionization in GaAs (circles) and GaN (squares). Adapted from [683]



at the moment of generation of secondary generated carriers depends linearly on the primary electron or hole energy.

The energy dependence of the electron initiated impact ionization rate has been calculated for GaAs, GaN and ZnS considering details and anisotropy of the band structure in [683]. The rates averaged over the Brillouin zone are compared in Fig. 8.17. Because of the large band gap of GaN, impact ionization can only be generated by electrons in higher conduction bands. The sharp increase of ionization rate for GaN around 5.75 eV correlates with a large valence band DOS from hole states at the zone boundary.

8.5 High-Frequency Transport

The above consideration pertained to dc (or slowly varying) fields. Now, we consider an ac field. It accelerates the carriers but at the same time the dissipative force in the relaxation-time approximation is present, i.e. (for electrons)

$$m^* \dot{\mathbf{v}} = -e \mathbf{E} - m^* \frac{\mathbf{v}}{\tau}. \quad (8.34)$$

For a harmonic field $E \propto \exp(-i\omega t)$ the complex conductivity ($\mathbf{j} = \sigma \mathbf{E} = nq\mathbf{v}$) is

$$\sigma = \frac{n e^2 \tau}{m^*} \frac{1}{1 - i\omega\tau} = \frac{n e^2}{m^*} \frac{i}{\omega + i\gamma}, \quad (8.35)$$

with $\gamma = 1/\tau$ being the damping constant. Splitting into real and imaginary parts yields

$$\sigma = \frac{n e^2 \tau}{m^*} \left(\frac{1}{1 + \omega^2 \tau^2} + i \frac{\omega \tau}{1 + \omega^2 \tau^2} \right). \quad (8.36)$$

For small frequencies ($\omega \rightarrow 0$) the dc conductivity from (8.5) is recovered, i.e. $\sigma = ne^2\tau/m^*$. For high frequencies ($\omega\tau \gg 1$)

$$\sigma = \frac{n e^2 \tau}{m^*} \left(\frac{1}{\omega^2 \tau^2} + i \frac{1}{\omega \tau} \right). \quad (8.37)$$

8.6 Polarons

In an ionic lattice, the electron polarizes the ions and causes a change of their equilibrium position. Depending of the severity of this effect, the lattice polarization leads to a modification of carrier (electron or hole) mass during band transport (Sect. 8.6.1) (*large* polarons) or the lattice deformation is so strong that it leads to carrier localization on the length scale of the lattice constant. Such self-trapped carriers are termed *small* polarons and discussed in Sect. 8.6.1. Reviews are given in [684, 685].

8.6.1 Large Polarons

When the electron moves through the ionic crystal and must drag an ion displacement with it, the effective electron mass changes to the ‘polaron mass’ m_p ,⁴

⁴For the calculation, many-particle theory and techniques are needed; the best solution is still given by Feynman’s path integral calculation [686–688].

Table 8.5 Fröhlich coupling constant α for various semiconductors

GaSb	GaAs	GaP	GaN	InSb	InAs	InP	InN
0.025	0.068	0.201	0.48	0.022	0.045	0.15	0.24
3C-SiC	ZnO	ZnS	ZnSe	ZnTe	CdS	CdSe	CdTe
0.26	1.19	0.63	0.43	0.33	0.51	0.46	0.35

Data from [691]

$$m_p = m^* \left(1 + \frac{\alpha}{6} + 0.025 \alpha^2 + \dots \right), \quad (8.38)$$

for $\alpha \leq 1$, with m^* being the band mass as defined in Sect. 6.8.2 and α the Fröhlich coupling constant⁵

$$\alpha = \frac{1}{2} \frac{e^2}{\hbar} \sqrt{\frac{2 m^*}{\hbar \omega_{LO}}} \left(\frac{1}{\epsilon_\infty} - \frac{1}{\epsilon_0} \right). \quad (8.39)$$

This process is called the *polaronic* effect and requires additional energy [686, 689]. Often, the polaron mass is given as $m_p = m^*/(1 - \alpha/6)$ which is the result of perturbation theory [689] and an approximation to (8.38) for small α .

For large coupling parameter, $\alpha \gg 1$, the polaron mass is given by [687]

$$m_p = m^* \frac{16}{81 \pi^4} \alpha^4. \quad (8.40)$$

The energy of the electron is lowered due to the interaction with the lattice. The energy E_0 for $k = 0$ is given, relative to the uncoupled case, by

$$E_0 = -(\alpha + 0.0098 \alpha^2 + \dots) \hbar \omega_0, \quad \alpha \leq 1 \quad (8.41a)$$

$$E_0 = -(2.83 + 0.106 \alpha^2) \hbar \omega_0, \quad \alpha \gg 1 \quad (8.41b)$$

Numerical results are reported in [690].

Polarons in semiconductors are typically ‘large’ or Fröhlich-type polarons, i.e. the coupling constant is small (Table 8.5). The dressing with phonons (as the ion displacement is called in a quantum-mechanical picture) is then only a perturbative effect and the number of phonons per electron ($\approx \alpha/2$) is small. If α becomes large ($\alpha > 1$, $\alpha \sim 6$), as is the case for strongly ionic crystals such as alkali halides, the polaron becomes localized by the electron–phonon interaction⁶ and hopping occurs infrequently from site to site.

⁵This constant is part of the matrix element in the Hamiltonian of the electron–phonon interaction and is related to the electric field created by LO phonons, as given in (5.52).

⁶One can think about it in the way that the electron strongly polarizes the lattice and digs itself a potential hole out of which it can no longer move.

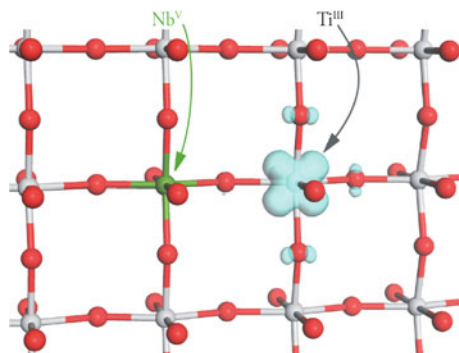


Fig. 8.18 Hole from Nb acceptor localized on Ti site (small polaron) in rutile TiO_2 . Adapted from [694]

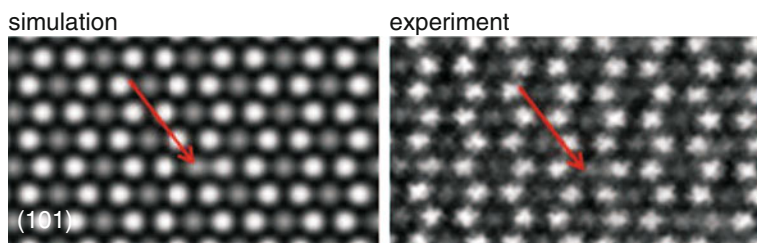


Fig. 8.19 Simulated and experimental TEM images of $\beta\text{-Ga}_2\text{O}_3$ in (101) projection. The *arrow* denotes the position of a polaron. Adapted from [693]

8.6.2 Small Polarons

In a polaron, the charge carrier (electron or hole) sits in a potential well resulting from the ionic displacements it created. In some materials, the shape and strength of this potential well is such that the charge is confined to a volume of approximately one unit cell or less. In this case, the polaron is called a small polaron. An example of a hole polaron in rutile $\text{TiO}_2\text{:Nb}$ is depicted in Fig. 8.18. In oxides often the hole from an acceptor is bound to oxygen, e.g. in $\text{BaTiO}_3\text{:Na}$, as reviewed in [692]. In Fig. 8.19 the lattice relaxation due to a hole bound to oxygen in the monoclinic unit cell of $\beta\text{-Ga}_2\text{O}_3$ is depicted directly using aberration corrected TEM. The bonding of the hole to the oxygen atom breaks the bond to a Ga atom which moves by 0.1 nm from its equilibrium position [693].

A proper theoretical analysis of a small polaron requires ab initio techniques that account for the motion of each atom in the few unit cells nearest the electron.⁷

The transport of small polarons occurs generally via thermally-activated hopping (cmp. Sect. 8.7). Under certain conditions the following mobilities for drift and Hall

⁷This paragraph has been taken from the concise tutorial by S.J.F. Byrnes [695].

effect have been given [684]:

$$\mu_d \propto T^{-1} \exp(-W/(2kT)), \tag{8.42}$$

$$\mu_H \propto T^{-1/2} \exp(-W/(6kT)), \tag{8.43}$$

W being the polaron binding energy. Generally, materials with small polar on transport exhibit high carrier density, often due to structural defects, and low mobility.

8.7 Hopping Transport

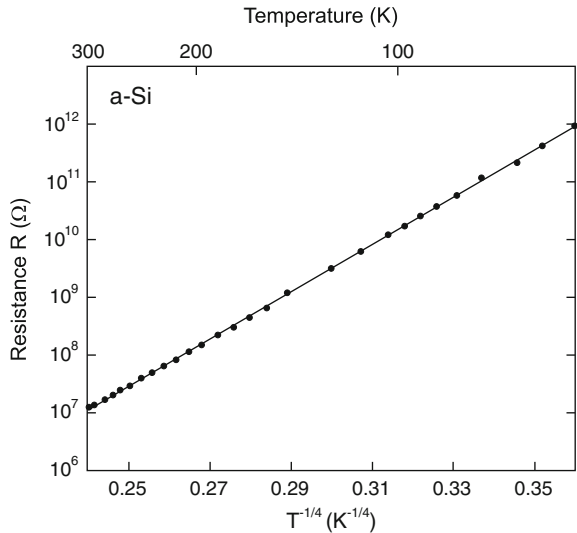
Disordered solids such as amorphous semiconductors, films containing quantum dots or material with many defects are characterized by a large density of localized states which can form band tails or a large density of states within the band gap. Hopping conduction is the tunneling between localized states and has been treated with various models [696–698].

A commonly observed phenomenon is the variable range hopping with a conductivity given by

$$\sigma = \sigma_0 \exp(-(T_0/T)^s) \tag{8.44}$$

with $s = 1/4$. Such law is fulfilled for amorphous silicon (Fig. 8.20). Mott has derived [700] and the exponent $s = 1/4$ using the following argument: The probability p to

Fig. 8.20 Temperature dependence of the planar resistance for Si films deposited at room temperature. *Solid line* is linear fit with $T_0 = 8 \times 10^7$ K according to (8.44) ($s = 1/4$). Adapted from [699]



hop from one localized site to another is proportional to

$$p \propto \exp(-2\alpha R - W/kT). \quad (8.45)$$

The first term stems from the probability to find the electron within radius R from its initial site, α being the decay constant of its wave function, $\Psi(r) \propto \exp(-\alpha r)$. The second term is the Boltzmann factor for bridging the energy mismatch W between localized states with a phonon-assisted process, assuming a low temperature limit ($kT \ll W$). There is a trade-off between hopping to levels closer in energy but spatially further away (on average), preferred at low temperature and the hopping to energy levels with larger W but spatially closer at higher temperatures. Thus the hopping range changes with temperature, giving the mechanism its name.

$D(E_F)$ shall be the (constant) density of localized states around the Fermi level. Within a radius R , there is on average one state of energy between 0 and $W(R)$ when (for three-dimensional bulk material)

$$W(R) = \frac{1}{D(E_F) (4\pi/3) R^3}. \quad (8.46)$$

Substituting (8.46) in (8.44) and searching for the maximum yields the most probable hopping distance

$$R \approx (\alpha kT D(E_F))^{-1/4}, \quad (8.47)$$

showing again, the varying range of hopping with temperature. Thus we find for T_0 in (8.44),

$$T_0 \approx \frac{\alpha^3}{k D(E_F)}. \quad (8.48)$$

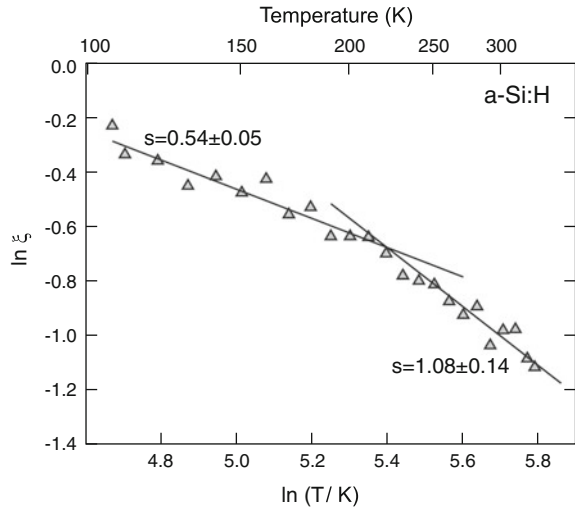
Other types of hopping mechanisms are the Efros–Shklovskii variable range hopping ($s = 1/2$), emerging for an energy dependent density of states $D(E) \propto (E - E_F)^2$ due to Coulomb interaction between hopping sites [701], or the next neighbor hopping ($s = 1$).

From (8.44) one can rewrite for $\xi = d(\ln \sigma(T))/d \ln T$,

$$\ln \xi = \ln s + s \ln T_0 - s \ln T. \quad (8.49)$$

Thus in a plot of $\ln \xi$ versus $\ln T$, the exponent s can be determined from the slope. As can be seen in Fig. 8.21, for the conductivity of a hydrogenated amorphous silicon thin film the transition of hopping mechanism from Efros–Shklovskii variable range hopping ($s \approx 1/2$) to next neighbor hopping ($s \approx 1$) takes place around $T = 220$ K, as discussed in detail in [702].

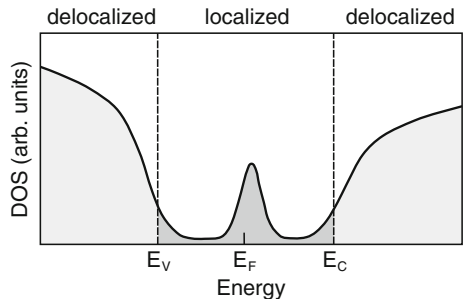
Fig. 8.21 Temperature dependence of conductivity of a hydrogenated amorphous Si thin film, plotted as $\ln \xi$ versus $\ln T$ (8.49). Solid lines are linear fits for constant s according to (8.49) as labelled. Adapted from [702]



8.8 Transport in Amorphous Semiconductors

Many models have been presented for the carrier transport in amorphous semiconductors [178]. The most important concept is that of a *mobility edge*, an energy separating localized from delocalized states [475, 476, 703]. This is schematically depicted in Fig. 8.22. The carrier transport between localized states is mediated via tunneling (hopping) which has been described in the previous section (Sect. 8.7). The localization of carriers in random lattices has been treated by Anderson [560] and reviewed in [558]. If the degree of disorder surpasses a certain value, diffusion is suppressed (at $T = 0$) and conductivity vanishes altogether (Anderson metal–insulator transition).

Fig. 8.22 Schematic density of states of amorphous semiconductor with band tails and deep levels. The localized (delocalized) states are shown in dark (light) grey. The mobility edges for electrons and holes are indicated by dashed lines



The transport in delocalized states is similar to band transport. The conductivity (for electrons) is given as

$$\sigma = -e \int_{E_C}^{\infty} D_e(E) \mu_e(E) f_e(E) dE. \quad (8.50)$$

If the Fermi energy is close to the middle of the gap, pinned to deep states, the Fermi-Dirac distribution can be replaced by the Boltzmann factor. Assuming a constant density of states and mobility for the delocalized states,

$$\sigma = -e D_e(E_C) \mu_e(E_C) kT \exp\left(\frac{E_C - E_F}{kT}\right). \quad (8.51)$$

Charge carriers from localized states in the tails can be thermally excited into delocalized states and contribute to conductivity (thermally activated hopping). The mobility then contains an exponential thermal activation term [178].

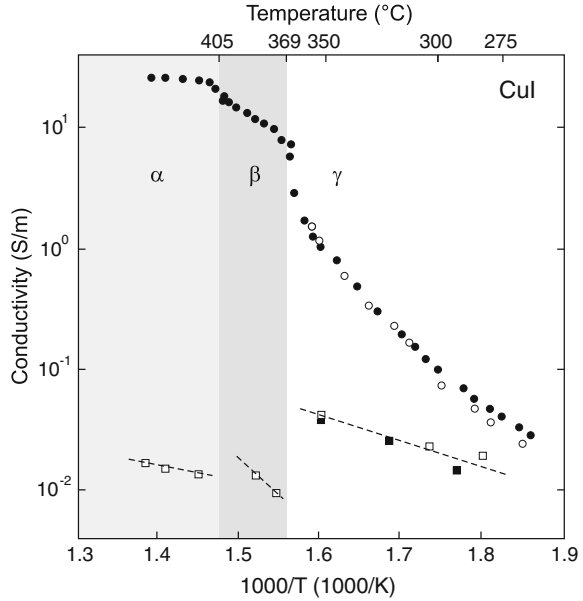
8.9 Ionic Transport

Ionic transport is the movement of ions upon application of a voltage. Here, we discuss only solid electrolytes. The transport can include the motion of one or several of the constituents of the lattice and the transport of other ions (e.g. hydrogen ions (protons), oxygen ions) through the crystal. Related to this is the diffusive ionic movement of impurities or defects through the crystal (cmp. Sect. 4.2.3). Ionic conduction of the lattice constituents under dc voltage will eventually destroy the crystal.

In typical semiconductors like silicon or gallium arsenide, the conductivity is entirely due to electronic conduction. A typical solid electrolyte is zirconia (ZrO_2) doped with yttria, so-called yttria-stabilized zirconia (YSZ) that takes on a cubic fluorite lattice (see Sect. 3.4.8). It can conduct oxygen ions via the mobility of oxygen vacancies for use in solid-oxide fuel cells (SOFC) [704]. The conductivity is about 0.01 S/cm at a temperature around 1000 K, almost entirely due to ionic transport. Doping with calcium oxide results in an oxygen conductor that is used in oxygen sensors in automobiles (lambda sensor). The ionic conductivity can be significantly increased, compared to bulk material, along interfaces [705, 706].

Other typical solid electrolytes are cuprous iodide (CuI) [494] and also AgI. In the high temperature cubic phase (α -polymorph), the iodide ions form a fairly rigid cubic framework and the metal ions are mobile; the copper diffusion pathways have been discussed [707, 708]. The temperature dependence of conductivity of CuI is shown in Fig. 8.23.

Fig. 8.23 Total (circles) and electronic (squares) conductivity of CuI coexisting with copper. Filled (empty) symbols refer to polycrystalline (single crystal) samples. The different structural phases (α (cubic), β (wurtzite), γ (zincblende)) are indicated by shaded areas as labeled. Dashed lines are guides to the eyes. Adapted from [709]



8.10 Diffusion

A gradient of a particle concentration n leads to a particle current proportional to $-\nabla n$. This diffusion law (Fick’s law) corresponds microscopically to a random walk. The gradients of the semiconductor carrier densities ∇n or ∇p thus lead to electron and hole currents, respectively:

$$\mathbf{j}_n = eD_n \nabla n \tag{8.52a}$$

$$\mathbf{j}_p = -eD_p \nabla p. \tag{8.52b}$$

The coefficients D_n and D_p are called the electron and hole diffusion coefficient, respectively. Thus the total electron and hole currents in the presence of an electric field \mathbf{E} and diffusion are

$$\mathbf{j}_n = -e\mu_n n \mathbf{E} + eD_n \nabla n \tag{8.53a}$$

$$\mathbf{j}_p = e\mu_p p \mathbf{E} - eD_p \nabla p. \tag{8.53b}$$

This relation can also be deduced more generally from the gradient of the Fermi level as

$$\mathbf{j}_n = -e\mu_n n \mathbf{E} - n\mu_n \nabla E_F \tag{8.54a}$$

$$\mathbf{j}_p = e\mu_p p \mathbf{E} - p\mu_p \nabla E_F. \tag{8.54b}$$

Using (7.6) and (7.7) for the concentrations (valid also in the case of degeneracy) and using $dF_j(x)/dx = F_{j-1}(x)$ we obtain

$$\mathbf{j}_n = -e\mu_n n \mathbf{E} - kT \mu_n \frac{F_{1/2}(\eta)}{F_{-1/2}(\eta)} \nabla n \quad (8.55a)$$

$$\mathbf{j}_p = e\mu_p p \mathbf{E} - kT \mu_p \frac{F_{1/2}(\zeta)}{F_{-1/2}(\zeta)} \nabla p, \quad (8.55b)$$

with $\eta = (E_F - E_C)/kT$ and $\zeta = -(E_F - E_V)/kT$. If the pre-factor of the density gradient is identified as the diffusion coefficient we find the (generalized) so-called ‘Einstein relations’ ($\beta = e/(kT)$) [529, 710]:

$$D_n = -\beta^{-1} \mu_n \frac{F_{1/2}(\eta)}{F_{-1/2}(\eta)} \quad (8.56a)$$

$$D_p = \beta^{-1} \mu_p \frac{F_{1/2}(\zeta)}{F_{-1/2}(\zeta)}. \quad (8.56b)$$

Useful analytical approximations have been discussed in [711]. We note that, e.g., (8.56a) can also be written as [712, 713]

$$D_n = -\beta^{-1} \mu_n n \frac{\partial \eta}{\partial n}. \quad (8.57)$$

In the case of nondegeneracy, i.e. when the Fermi level is within the band gap and not closer than about $4kT$ to the band edges, $\eta = \ln(n/N_C)$. Then $\partial \eta / \partial n = 1/n$, and the equation simplifies to $D = (kT/q) \mu$, i.e. the ‘regular’ Einstein-relations,

$$D_n = -\beta^{-1} \mu_n \quad (8.58a)$$

$$D_p = \beta^{-1} \mu_p. \quad (8.58b)$$

In this case, (8.53a,b) read

$$\mathbf{j}_n = -e\mu_n n \mathbf{E} - kT \mu_n \nabla n \quad (8.59a)$$

$$\mathbf{j}_p = e\mu_p p \mathbf{E} - kT \mu_p \nabla p. \quad (8.59b)$$

We recall that both diffusion coefficients are positive numbers, since μ_n is negative. Generally, the diffusion coefficient depends on the density. A Taylor series of the Fermi integral yields

$$D_n = -\beta^{-1} \mu_n \left[1 + 0.35355 \left(\frac{n}{N_C} \right) - 9.9 \times 10^{-3} \left(\frac{n}{N_C} \right)^2 + \dots \right]. \quad (8.60)$$

8.11 Continuity Equation

The balance equation for the charge is called the continuity equation. The temporal change of the charge in a volume element is given by the divergence of the current and any source (generation rate G), e.g. an external excitation, or drain (recombination rate U). Details about recombination mechanisms are discussed in Chap. 10. Thus, we have

$$\frac{\partial n}{\partial t} = G_n - U_n - \frac{1}{q} \nabla \cdot \mathbf{j}_n = G_n - U_n + \frac{1}{e} \nabla \cdot \mathbf{j}_n \quad (8.61a)$$

$$\frac{\partial p}{\partial t} = G_p - U_p - \frac{1}{e} \nabla \cdot \mathbf{j}_p. \quad (8.61b)$$

In the case of nondegeneracy we find, using (8.53a,b)

$$\frac{\partial n}{\partial t} = G_n - U_n - \mu_n n \nabla \cdot \mathbf{E} - \mu_n \mathbf{E} \nabla n + D_n \Delta n \quad (8.62a)$$

$$\frac{\partial p}{\partial t} = G_p - U_p - \mu_p p \nabla \cdot \mathbf{E} - \mu_p \mathbf{E} \nabla p + D_p \Delta p. \quad (8.62b)$$

In the case of zero electric field these read

$$\frac{\partial n}{\partial t} = G_n - U_n + D_n \Delta n \quad (8.63a)$$

$$\frac{\partial p}{\partial t} = G_p - U_p + D_p \Delta p, \quad (8.63b)$$

and if the stationary case also applies:

$$D_n \Delta n = -G_n + U_n \quad (8.64a)$$

$$D_p \Delta p = -G_p + U_p. \quad (8.64b)$$

8.12 Heat Conduction

We consider here the heat transport [714] due to a temperature gradient. The heat flow \mathbf{q} , i.e. energy per unit area per time in the direction $\hat{\mathbf{q}}$, is proportional to the local gradient of temperature. The proportionality constant κ is called, heat conductivity,

$$\mathbf{q} = -\kappa \nabla T. \quad (8.65)$$

In crystals, the heat conductivity can depend on the direction and thus κ is generally a tensor of rank 2. In the following, κ will be considered as a scalar quantity. The quite generally valid Wiedemann–Franz law connects the thermal and electrical

conductivities

$$\kappa = \frac{\pi^2}{3} \left(\frac{k}{e}\right)^2 T \sigma. \tag{8.66}$$

The balance (continuity) equation for the heat energy Q is

$$\nabla \cdot \mathbf{q} = -\frac{\partial Q}{\partial t} = -\rho C \frac{\partial T}{\partial t} + A, \tag{8.67}$$

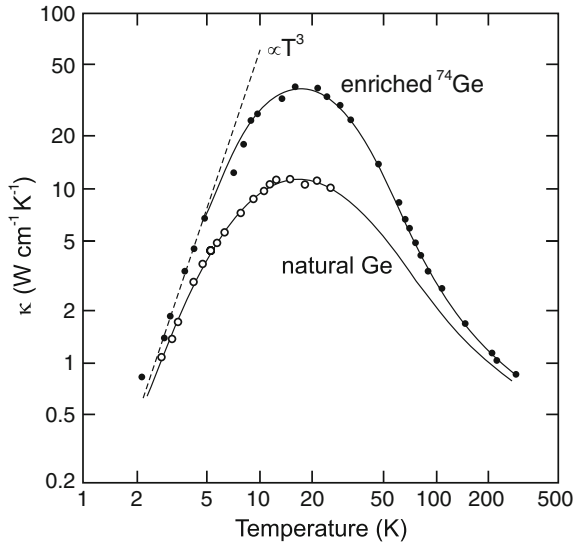
where ρ denotes the density of the solid and C the heat capacity. A denotes a source or drain of heat, e.g. an external excitation. Combining (8.65) and (8.67), we obtain the equation for heat conductivity

$$\Delta T = \frac{\rho C}{\kappa} \frac{\partial T}{\partial t} - \frac{A}{\kappa}, \tag{8.68}$$

which simply reads $\Delta T = 0$ for a stationary situation without sources.

The random mixture of various atoms in natural elements represents a perturbation of the perfectly periodic lattice. Since the mass of the nuclei varies, in particular lattice vibrations will be perturbed. Thus we expect an effect on the heat conductivity. In Fig. 8.24, the thermal conductivity of crystals from natural Ge and enriched ^{74}Ge are compared [715], the latter having, as expected, the higher heat conductivity, i.e. less scattering. The thermal conductivity of isotopically pure ^{28}Si thin films has been measured to be 60% greater than natural silicon at room temperature and at least 40% greater at 100°C, a typical chip operating temperature [716, 717].

Fig. 8.24 Thermal conductivity of Ge versus temperature. The enriched Ge consists of 96% ^{74}Ge while the natural isotope mix is 20% ^{70}Ge , 27% ^{72}Ge , 8% ^{73}Ge , 27% ^{74}Ge and 8% ^{76}Ge . The dashed line shows the $\kappa \propto T^3$ dependence at low temperatures (Debye's law). Adapted from [715]



8.13 Coupled Heat and Charge Transport

The standard effect of coupled charge and heat transport is that a current heats its conductor via Joule heating. However, more intricate use of thermoelectric effects can also be employed to cool certain areas of a device. For further details see [718, 719].

For the analysis of coupled charge and heat transport we first sum the electric field and the concentration gradient to a new field $\hat{\mathbf{E}} = \mathbf{E} + \nabla E_F/e$. Then, the heat flow and charge current are

$$\mathbf{j} = \sigma \hat{\mathbf{E}} + L \nabla T \quad (8.69)$$

$$\mathbf{q} = M \hat{\mathbf{E}} + N \nabla T, \quad (8.70)$$

where $\hat{\mathbf{E}}$ and ∇T are the stimulators for the currents. From the experimental point of view there is interest to express the equations in \mathbf{j} and ∇T since these quantities are measurable. With new coefficients they read

$$\hat{\mathbf{E}} = \rho \mathbf{j} + S \nabla T \quad (8.71)$$

$$\mathbf{q} = \Pi \mathbf{j} - \kappa \nabla T, \quad (8.72)$$

where ρ , S and Π are the specific resistance, thermoelectric power and Peltier coefficient (transported energy per unit charge), respectively. The relations with the coefficients σ , L , M , and N are given by

$$\rho = \frac{1}{\sigma} \quad (8.73a)$$

$$S = -\frac{L}{\sigma} \quad (8.73b)$$

$$\Pi = \frac{M}{\sigma} \quad (8.73c)$$

$$\kappa = \frac{ML}{\sigma} - N. \quad (8.73d)$$

8.13.1 Thermopower and Seebeck Effect

A semiconductor shall have two ends at different temperatures T_2 and T_1 and a temperature gradient in between in an open circuit, i.e. $\mathbf{j} = 0$. Then a field $\hat{\mathbf{E}} = S \nabla T$ and a voltage $U = S/(T_2 - T_1)$ will arise. This effect is called the thermoelectric or Seebeck effect. S is termed the Seebeck coefficient or the *thermoelectric power*, often also denoted as Q in the literature. The voltage can be measured and used to determine the temperature at one end if the temperature at the other end is known, forming a thermometer. The Seebeck coefficient is positive if the electric field is in the same direction as the temperature gradient.

A famous relation from irreversible thermodynamics connects it to the Peltier coefficient via

$$S = \frac{\Pi}{T}. \tag{8.74}$$

The Seebeck coefficient is related to the energy transport by charge carriers. The heat (energy) flow is obviously from the hot to the cold end (assuming here $T_2 > T_1$), so is the flow of charge carriers. In a simple picture, if the energy is carried by (hot) holes, the current (by definition the direction of positive charge carriers) is from the hot to the cold end ($2 \rightarrow 1$); if the energy flow is carried by electrons, the current flows from the cold to the hot end ($1 \rightarrow 2$). Accordingly, energy transport by electrons and holes gives rise to different signs of the thermoelectric coefficient (Fig. 8.25). If the cold (unheated) substrate is grounded, the sign of the voltage at a hot solder tip pressed (carefully) on the surface of the semiconductor yields the conductivity type, n-type (p-type) for a negative (positive) voltage.

However, the semiconductor should not be heated so strongly that intrinsic conduction arises. In this case the conductivity and the thermoelectric power is determined by the carrier type with the higher mobility; typically, and for the case of silicon shown in Fig. 8.25, these are the electrons thus yielding a negative Seebeck coefficient in the intrinsic regime.

For band conduction the thermopower (I.29) is given for electrons (S_n) and holes (S_p) by [722] (for a derivation see Sect. I.4)

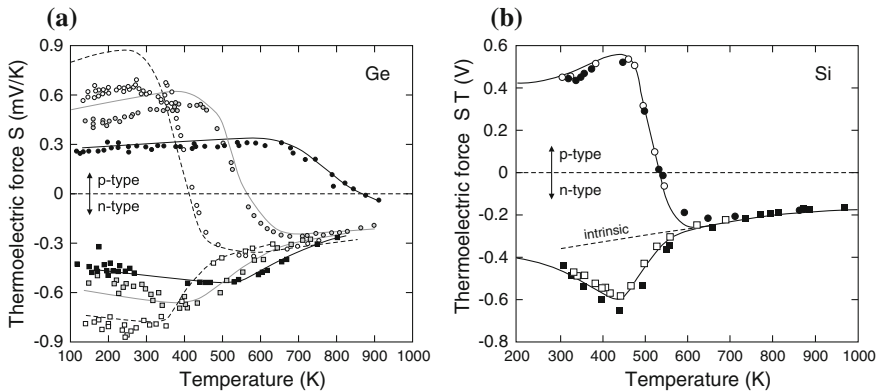


Fig. 8.25 (a) Seebeck coefficient S for n- and p-doped germanium. Experimental data (symbols) and theory (lines). $N_A - N_D$ is $5.7 \times 10^{15} \text{ cm}^{-3}$ (white circles), $1.7 \times 10^{17} \text{ cm}^{-3}$ (grey) and $7.2 \times 10^{18} \text{ cm}^{-3}$ (black); $N_D - N_A$ is $3.3 \times 10^{15} \text{ cm}^{-3}$ (white squares), $1.1 \times 10^{17} \text{ cm}^{-3}$ (grey) and $6.2 \times 10^{17} \text{ cm}^{-3}$ (black) Adapted from [720]. (b) Thermoelectric force Π of lowly doped n- and p-silicon as a function of temperature. Solid line is from simple model calculation and symbols represent data from silicon samples with the approximate doping of circles: $1 \times 10^{15} \text{ cm}^{-3}$ B, $2 \times 10^{14} \text{ cm}^{-3}$ donors, squares $4 \times 10^{14} \text{ cm}^{-3}$ P, $9 \times 10^{13} \text{ cm}^{-3}$ acceptors. Adapted from [721]

$$S_n = -\frac{k}{e} \left(\frac{E_C - E_F}{kT} + A_C \right) \quad (8.75a)$$

$$S_p = \frac{k}{e} \left(\frac{E_F - E_V}{kT} + A_V \right), \quad (8.75b)$$

where A_i are constants (I.31a) depending on the energy dependence of the density of states and the mobility. The sign of the thermopower tells whether conduction takes place above (negative sign) or below (positive sign) the Fermi level.

If the Fermi level is fixed and both electrons and holes contribute (two-band conduction), the thermopower is (evaluating (I.32), $b = \sigma_n/\sigma_p$ and the gap center energy $E_M = (E_C - E_V)/2$)

$$S = \frac{k}{e} \left(\frac{1-b}{1+b} \frac{E_g}{2kT} + \frac{E_F - E_M}{kT} + \frac{A_V - b A_C}{1+b} \right). \quad (8.76)$$

In the case of intrinsic conduction from (7.18) $E_F - E_M = (kT/2) \ln(N_V/N_C)$.

The thermoelectric power from some highly doped n-type silicon samples is depicted in Fig. 8.26a. At low temperature the (low) conductivity is due to conduction in a donor impurity band (cmp. Sect. 7.5.7). At high compensation of about 90% (grey data points in Fig. 8.26a), the band is only 10% filled and acts like a valence band with positive thermopower at sufficiently low temperature when the free carrier density is small. Without compensation, the thermopower remains negative since the almost completely filled impurity band acts conduction band like. The dependence of thermopower on doping has been simulated in [723] (Fig. 8.26); the

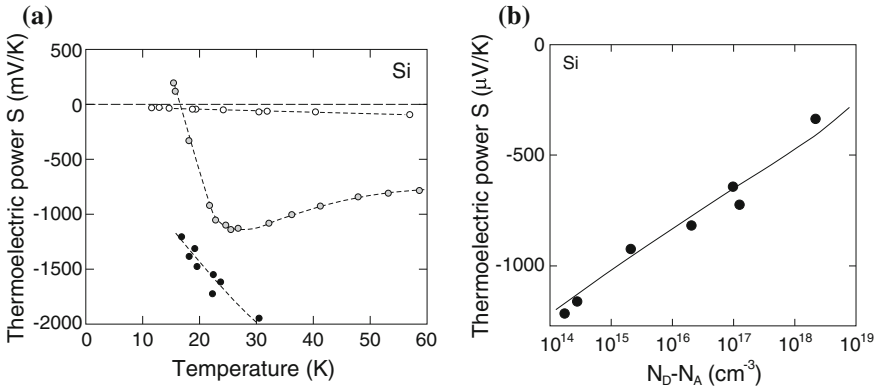


Fig. 8.26 (a) Thermoelectric power S of highly doped n-type silicon as a function of temperature. Circles are experimental data and dashed lines guides to the eyes. The approximate doping of the samples is white $2.7 \times 10^{19} \text{ cm}^{-3}$ As, grey $2.2 \times 10^{18} \text{ cm}^{-3}$ As, black $1.1 \times 10^{18} \text{ cm}^{-3}$ As and $1.0 \times 10^{18} \text{ cm}^{-3}$ B with $N_D - N_D = 1.25 \times 10^{17} \text{ cm}^{-3}$ at room temperature. Adapted from [721]. (b) Thermopower of doped n-type silicon at room temperature as a function of doping concentration. Experimental data (symbols) from [721] and theory (solid line) from [723]

decrease with increasing doping is mostly attributed to the reduced mobility due to ionized impurity scattering. The increase of thermopower at low temperatures is due to the *phonon-drag* effect which is discussed for the samples from [721] in [724].

As a figure of merit for the production of thermoelectric power the ZT -value is used, $ZT = \sigma S^2 T / \kappa$.

8.13.2 Peltier Effect

In a semiconductor with a temperature difference at its ends a current flow will be allowed now (short circuit). The current leads via the charge transport also to a heat (or energy) transport. This effect is called the Peltier effect. The Peltier coefficient is negative (positive) for electrons (holes). The total amount of energy P that is transported consists of the generation term and the loss due to transport:

$$P = \mathbf{j} \cdot \hat{\mathbf{E}} - \nabla \cdot \mathbf{q}. \tag{8.77}$$

With (8.71) and (8.72) we find

$$P = \frac{\mathbf{j} \cdot \mathbf{j}}{\sigma} + S \mathbf{j} \cdot \nabla T - \Pi \nabla \cdot \mathbf{q} + \kappa \Delta T. \tag{8.78}$$

The first term is Joule heating, the second term is Thomson heating. The third exists only when carriers are generated or when they recombine. The fourth term is the heat conduction. In the Thomson term $S \mathbf{j} \cdot \nabla T$ heat is generated in an n-type semiconductor if \mathbf{j} and ∇T are in the same direction. This means that electrons that move from the hotter to the colder part transfer energy to the lattice. The effect can be used to construct a thermoelectric cooler, as shown in Fig. 8.27, that generates a temperature difference due to a current flow. For optimal performance σ should be large to prevent excess Joule heating and κ should be small such that the generated temperature difference is not rapidly equalized.

Fig. 8.27 Schematic Peltier cooler. The heat sinks (grey) and the cold junction (black) on the left are metals that make ohmic contacts with the semiconductors. The current flow is such that electrons move through the n-type semiconductor from right to left

